Stem Cell Reports
Article

ISSCR

OPEN ACCESS

Embryonic stem cell ERK, AKT, plus STAT3 response dynamics combinatorics are heterogeneous but NANOG state independent

Andreas Reimann,[1,2,4] Tobias Kull,[1,4] Weijia Wang,[1] Philip Dettinger,[1] Dirk Loeffler,[1,3] and Timm Schroeder[1,*]
[1]Department of Biosystems Science and Engineering, ETH Zurich, 4058 Basel, Switzerland
[2]Present address: Ichnos Sciences Biotherapeutics SA, 1066 Epalinges, Switzerland
[3]Present address: Department of Hematology, St. Jude Children's Research Hospital, Memphis, TN 38105, USA
[4]These authors contributed equally
*Correspondence: timm.schroeder@bsse.ethz.ch
https://doi.org/10.1016/j.stemcr.2023.04.008

SUMMARY

Signaling is central in cell fate regulation, and relevant information is encoded in its activity over time (i.e., dynamics). However, simultaneous dynamics quantification of several pathways in single mammalian stem cells has not yet been accomplished. Here we generate mouse embryonic stem cell (ESC) lines simultaneously expressing fluorescent reporters for ERK, AKT, and STAT3 signaling activity, which all control pluripotency. We quantify their single-cell dynamics combinations in response to different self-renewal stimuli and find striking heterogeneity for all pathways, some dependent on cell cycle but not pluripotency states, even in ESC populations currently assumed to be highly homogeneous. Pathways are mostly independently regulated, but some context-dependent correlations exist. These quantifications reveal surprising single-cell heterogeneity in the important cell fate control layer of signaling dynamics combinations and raise fundamental questions about the role of signaling in (stem) cell fate control.

INTRODUCTION

Embryonic stem cells (ESCs) have unlimited self-renewal and pluripotent lineage potential. Defined *in vitro* conditions supporting self-renewal as well as differentiation (Ying et al., 2008), fast proliferation, and easy genetic manipulation (Chambers et al., 2003; Hastreiter et al., 2018) make ESCs a perfect model system for mammalian systems biology and for analyzing molecular stem cell fate control. ESC self-renewal and differentiation into specific lineages is regulated by culture conditions influencing the activity of signaling pathways (Chen et al., 2015; Kim et al., 2012; Ying et al., 2008). Signaling thus is at the apex of their fate control, and its effects are mediated through downstream effectors including transcription factors and their networks (Filipczyk et al., 2015; Ng and Surani, 2011; Schulz et al., 2014). Signaling activity is heterogeneous between individual cells even upon identical stimulation of seemingly homogeneous populations (Kull and Schroeder, 2021; Singh et al., 2010). In addition, signaling pathways can not only be switched on or off in a binary fashion but can display different activity patterns over time (i.e., dynamics). These signaling dynamics can encode relevant information and control fate choices. For instance, sustained ERK signaling in PC12 cells leads to neural differentiation, while transient ERK activity triggers proliferation (Marshall, 1995; Ryu et al., 2015). In human hematopoietic stem cells, different ERK signaling dynamics correlate with different future fates (Wang et al., 2021), and oscillatory NFKB dynamics bias granulocyte-monocyte progenitors to the monocyte lineage (Kull et al., 2022). Signaling activity dynamics can only be recognized by continuous single-cell quantification (Endele and Schroeder, 2012; Etzrodt et al., 2014; Hoppe et al., 2014; Kull and Schroeder, 2021; Schroeder, 2005). Given the crosstalk between different signaling pathways, they should be analyzed simultaneously. However, this remains technically demanding, and most studies therefore only analyzed single signaling pathways mostly in easy-to-handle cell lines (Deathridge et al., 2019; Lane et al., 2017; Purvis et al., 2012; Ryu et al., 2015; Tay et al., 2010). Information about signaling dynamics and their combinatorics between different pathways in more complex mammalian stem cells therefore does not yet exist. ESCs allow to investigate complex combinatorial signaling dynamics due to their well-defined culture conditions and easy genetic manipulation. However, despite increased homogeneity and pluripotency in chemically defined media conditions such as 2i, clonal ESCs remain heterogeneous and switch between different transient states (Chambers et al., 2007; Filipczyk et al., 2015; Hastreiter et al., 2018). The underlying causes for this heterogeneity remain unclear. Many studies analyzed ESC heterogeneity at the transcriptome (Klein et al., 2015), epigenome (Graf and Stadtfeld, 2008; Marks et al., 2012), or transcription factor network levels (Chambers et al., 2007; Filipczyk et al., 2013, 2015; Hastreiter et al., 2018; Torres-Padilla and Chambers, 2014). Recent studies analyzed ERK signaling dynamics in pluripotent cells in the murine blastocyst (Simon et al., 2020) and *in vitro* under differentiation (Deathridge et al., 2019) and pluripotency (Raina et al., 2022) conditions. All of them find surprising heterogeneity in

ERK dynamics, conclude that a combination of niche factors and lineage commitment is responsible for the observed differences, and suggest that specific ERK signaling dynamics may reflect specific ESC states and/or induce specific ESC fates. Although highly relevant, these studies only analyze the ERK pathway in a low number of cells, potentially missing rare cell populations with specific dynamics and co-dependencies between different pathways.

Here, we therefore use long-term single-cell time-lapse imaging and tracking to quantify signaling activity dynamics as well as cellular and molecular dynamics of, e.g., ESC movement, morphology, cell cycle lengths, protein expression, and cellular kinship (Ahmed et al., 2022; Eilken et al., 2009; Filipczyk et al., 2015; Hilsenbeck et al., 2016; Hoppe et al., 2016; Loeffler et al., 2019, 2021; Rieger et al., 2009; Wang et al., 2021). We generate ESC reporter cell lines to simultaneously quantify the activity dynamics of multiple pluripotency-related signaling pathways in single mouse ESCs across different culture and stimulation conditions. We show complex heterogeneity at several levels of analysis, correlate combinatorial signaling dynamics to other cellular properties, and find striking relationships between signaling, cell cycle, and morphology.

RESULTS

Novel ESC reporter lines for simultaneous live single-cell quantification of activity dynamics of several signaling pathways

We generated mouse ESC lines simultaneously expressing live cell activity reporters for multiple signaling pathways controlling ESC fates. We selected previously published kinase translocation reporters (KTRs) for the MAPK/ERK (Regot et al., 2014) and PI3K/AKT (Gross and Rotwein, 2015) pathways, as well as a STAT3 fusion reporter (Herrmann et al., 2004), for our study. KTR sensors (ERK/AKT) consist of a specific kinase docking site, a nuclear localization (NLS), and a nuclear export signal (NES), as well as a fluorescent protein. When their pathways are activated, the respective kinases phosphorylate these sensors, de-/activating the NLS/NES, resulting in a translocation of the fluorescent reporter protein from the nucleus to the cytoplasm. In case of STAT3, pathway activity is reported by localization of the STAT3 fusion protein itself, which translocates from the cytoplasm to the nucleus upon activation. These reporters enable robust quantification of the fast signaling kinetics of their pathways, which are highly relevant in controlling ESC fates. Next, selected reporters and an iRFP713nucmem sequence (Filonov et al., 2011; Okita et al., 2004) for constitutive fluorescent nucleus labeling for segmentation were combined into a single expression construct (Figures 1A and S1A). Stable integration into R1 WT ESCs was achieved by the transposon-based piggyBac system (Yusa et al., 2011).

We confirmed functionality and specificity of the three reporters in the multi-reporter ESC line by time-lapse imaging (Figures 1B and 1C). Inhibitors PD0325901 (ERK), PF04691502 (AKT), and BAY2353 (STAT3) prevent activation of the respective pathway reporters after stimulation as expected and previously published (Lorusso et al., 2005; Yuan et al., 2011), showing that reporters indeed reflect correct pathway activity also in mouse ESCs (Figures S1G and S1H). 5 weeks post sorting, reporters were still expressed as at the beginning of culture in >95% of ESCs (Figure S1D). Proliferation rates, NANOG and SOX2 pluripotency marker expression (Filipczyk et al., 2013, 2015), and differentiation potential were similar between the lines and to parental wild-type R1 ESCs (Figures S1C, S1E, and S1F).

Signaling pathway responses and their combinations are highly heterogeneous between single self-renewing ESCs

We simultaneously quantified the signaling activity dynamics of ERK, AKT, and STAT3 signaling pathways, which are central to pluripotency control (Li et al., 2012; Niwa et al., 2009; Paling et al., 2004; Ying et al., 2008). They were quantified during switching between different commonly used media conditions all enforcing ESC self-renewal: 2i (Chir99021+ PD0325901) inhibits ERK (Hastreiter et al., 2018; Ying et al., 2008), 2i+LIF ("2iLIF," LIF = leukemia inhibition factor) activates ERK and STAT3 (Smith et al., 1988; Ying et al., 2008), LIF+BMP4 ("LIFBMP4," BMP4 = bone morphogenic protein 4) activates ERK and STAT3 (Li et al., 2012; Ying et al., 2003), and Serum+LIF ("SerumLIF," Serum = fetal calf serum [FCS]) activates ERK and STAT3 (Chambers et al., 2007; Ying et al., 2003). Individual medium components such as LIF or the inhibitors in 2i were not used individually as this would not maintain self-renewal. Cells were imaged first in "start medium" for 30 min for baseline acquisition and then for 120 min after switching to a different medium. Time-lapse image data were analyzed with a custom computational analysis pipeline that includes nuclear segmentation, single-cell tracking, total nuclear fluorescence quantification, normalization, and time series classification (Eilken et al., 2009; Filipczyk et al., 2015; Hilsenbeck et al., 2016, 2017). Cells were selected randomly without biasing for cellular properties. In the rare cases where an ESC died before the end of the movie, it was excluded from the dataset.

A total of 7,712 single ESCs were observed in 16 different media switch conditions, and the dynamics of each of their three signaling sensors were quantified simultaneously. To properly compare the actual signaling dynamics and not

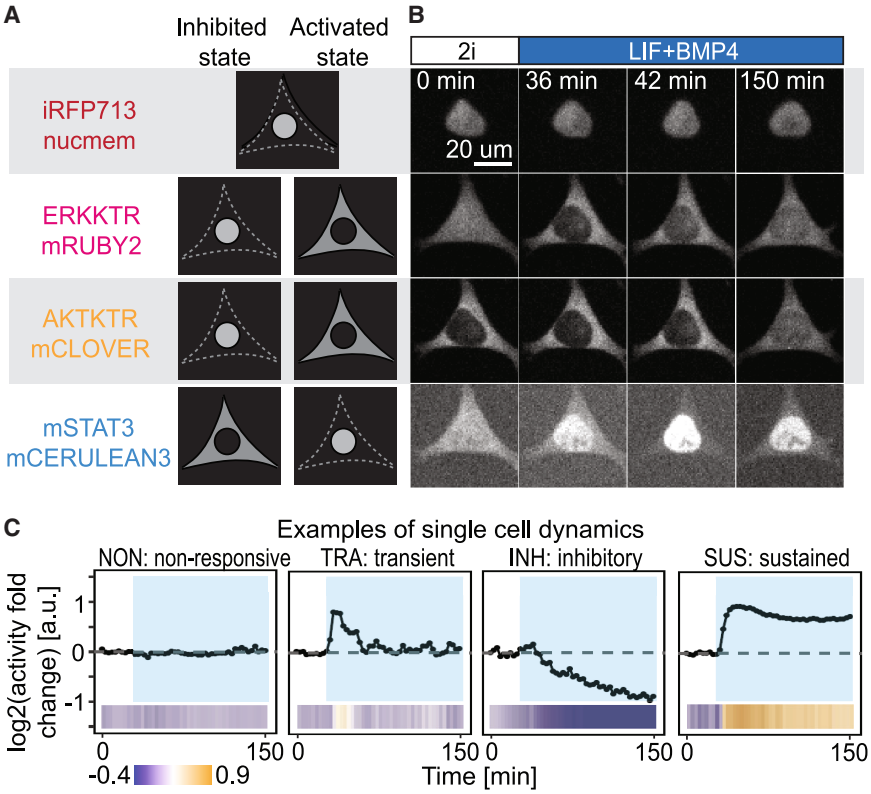

Figure 1. Continuous time-lapse imaging of quadruple reporter mESCs allows quantification of multiplexed signaling dynamics in live single ESCs

(A) Reporters and their signaling-activity-dependent subcellular localizations. Cytoplasmic ERK- and AKTKTR and nuclear STAT3 fusion proteins report pathway activity.

(B) Representative images of reporter protein localization changes upon ESC stimulation by switching self-renewal medium from 2i to LIFBMP4. Medium was switched 30 min after imaging start. An increase in activation for ERK and STAT3 can be observed.

(C) Quantification of single ESC signaling activity dynamics, with time series of log2 transformed fold changes of nuclear sensor fluorescence intensities relative to the baseline (activity before medium switch) average. Sensors were imaged and quantified every 180 s. Dynamics traces and "heat stripe" representations for different signaling dynamics are shown. Blue areas indicate time after medium switch (switch after 30 min). Sensor sensitivities are suitable for precise quantification and distinction of different dynamics patterns. See also Figure S1.

absolute sensor levels, every dynamics trace was normalized to its baseline before switching. This leads to a divergence of the signaling traces over time but normalizes for differences in single-cell biosensor expression. We found an unexpectedly large heterogeneity of dynamics at three different levels: between media switch conditions, between pathways and their combinations, and between individual ESCs within the same conditions (Figure 2A). ERK was most active in 2i-free conditions, as expected. AKT was highly activated upon serum removal, and STAT3 was strongly activated by LIF (Figures 2A and 2B). Adding LIF to 2i activated STAT3 but not AKT or ERK. Switching from 2iLIF to LIFBMP4 only activated ERK. As expected, the average signaling activity of the whole population did not alter when medium was switched to itself (i.e., no change in medium components), validating our approach (Figure 2A, diagonal; Figure S2C).

We found the same mean pathway responses to different stimuli as were previously described (Hastreiter et al., 2018; Li et al., 2012; Ying et al., 2003, 2008). However, responses massively varied between individual ESCs of a switch/pathway combination. Population averaging would thus miss true pathway activities, and individual cells from a mean non-responsive population could get activated even more than ESCs of a mean responding population. Surprisingly, considerable heterogeneity was present even between ESCs in culture conditions like 2i or 2iLIF that are assumed to reduce cell-to-cell variability (Hastreiter et al., 2018; Smith et al., 1988; Ying et al., 2008). To more precisely quantify the influence of the individual signaling modulators serum, LIF, 2i, and BMP4, conditions were sub-classified depending on whether a specific component was added, removed, or not changed. 2i was treated as a single medium component, since we did not examine the influence of CHIR99021 or PD0325901 individually as media with only one inhibitor do not maintain self-renewal. Responses were quantified for their area under the curve (AUC; reflects the total activation of a given pathway) and the persistence of their activity. In all categories, we observed an array of different responses with positive and negative AUCs indicating pathway activation and inhibition, respectively (Figure 2C). None of the used stimuli alone was sufficient to induce AKT signaling, but instead, a specific combination of stimuli was necessary. Effects on ERK and STAT3 on the other hand showed clear responses to specific individual medium components, regardless of the presence of other stimuli.

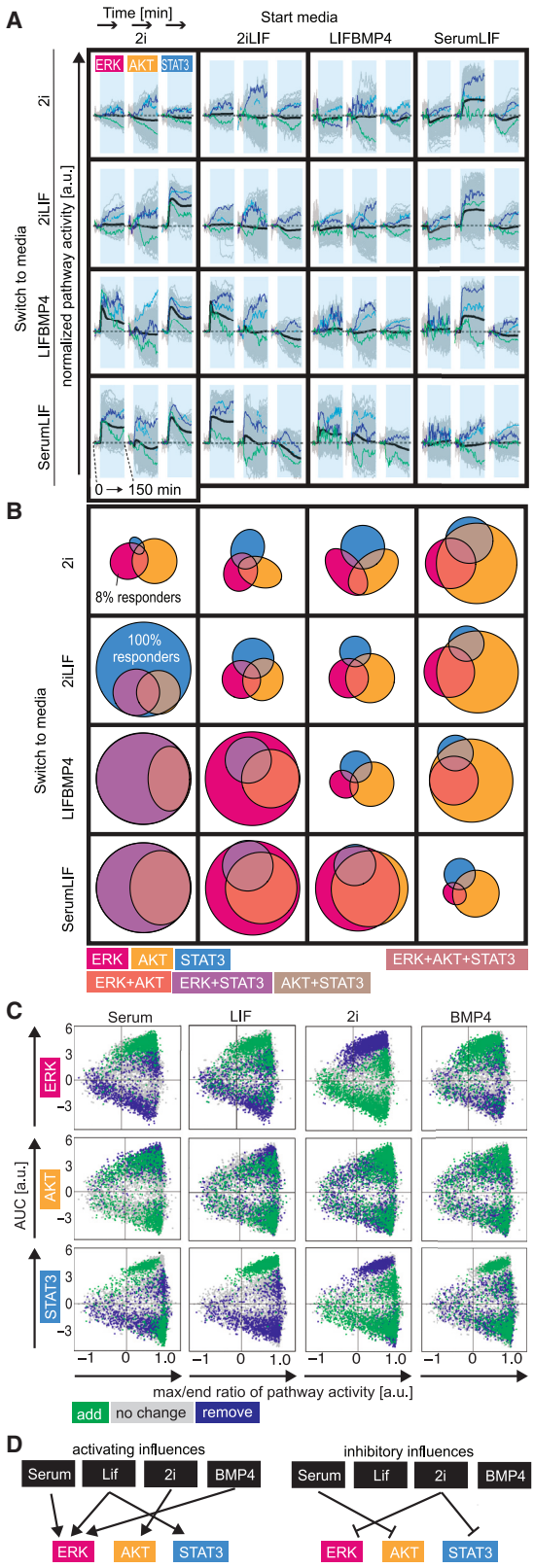

Figure 2. Signaling dynamics in ESCs are heterogeneous across stimulation conditions, pathways, and single ESCs

(A) Signaling dynamics traces for different pathways and stimulation conditions over 150 min. Gray lines: single ESCs, black lines: average. Colored lines: randomly selected exemplary single-cell traces. Shaded blue areas indicate time after medium switch (30 min post imaging start). Note the dynamics heterogeneities at several levels: across media conditions, pathways, and single ESCs.

(B) Percentages of responding ESCs (pathway activity above threshold after medium switch) for all pathways and stimulation conditions. Areas correspond to responding percentages. Response probabilities are very different for different stimulation conditions. Column labels are like in (A).

(C) Influence of media components on pathway activity (as reflected by the area under the curve [AUC] of each dynamics curve) and max/end ratio (high values indicate transient behavior) of all three pathways. Columns are as in (A). Color coding refers to conditions where the respective component is added (green), removed (blue), or not changed (gray). Positive and negative y axis values reflect pathway activation and inhibition, respectively. High and low x values suggest transient and sustained signaling activation, respectively. Effects of serum, LIF, 2i, or BMP4 on AKT are more heterogeneous than on ERK or STAT3.

(D) Summary of data from (C). N = 3 independent samples (cell populations) measured in 12 independent experiments. See also Figure S2.

Even though all four media conditions support ESC self-renewal and inhibit differentiation, they have very different influences on ESC signaling. Confirming average responses and in agreement with previous studies, LIF was the strongest activator of STAT3 (Smith et al., 1988). BMP4 and serum had similar activating effects on ERK and STAT3, further supporting earlier studies that claim BMP4 to be the main serum component responsible for ESC self-renewal (Ying et al., 2003). Removal of serum in any media type resulted in a sharp and sustained AKT activity increase, confirming serum as an inhibitor of AKT signaling. Interestingly, the addition of serum can also lead to transiently increased AKT activity in some cases, suggesting that only longer exposure results in inhibition (Figure 2C). This has not been shown so far and would be easily missed by snapshot analyses. As expected, 2i was a strong inhibitor of ERK (Figure 2D).

Correlation of dynamics between signaling activity pathways is context dependent

We next analyzed ESC signaling behavior over time: the signaling dynamics. ESCs respond either with sustained (SUS), transient (TRA), or inhibitory (INH, negative) dynamics or are non-responsive (NON) (Figure 1B). We implemented a thresholding approach to objectively classify single ESC signaling dynamics (see supplemental methods for details).

Similar behavior of all ESCs could be observed before stimulation (first 10 time points; 0–30 min) regardless of

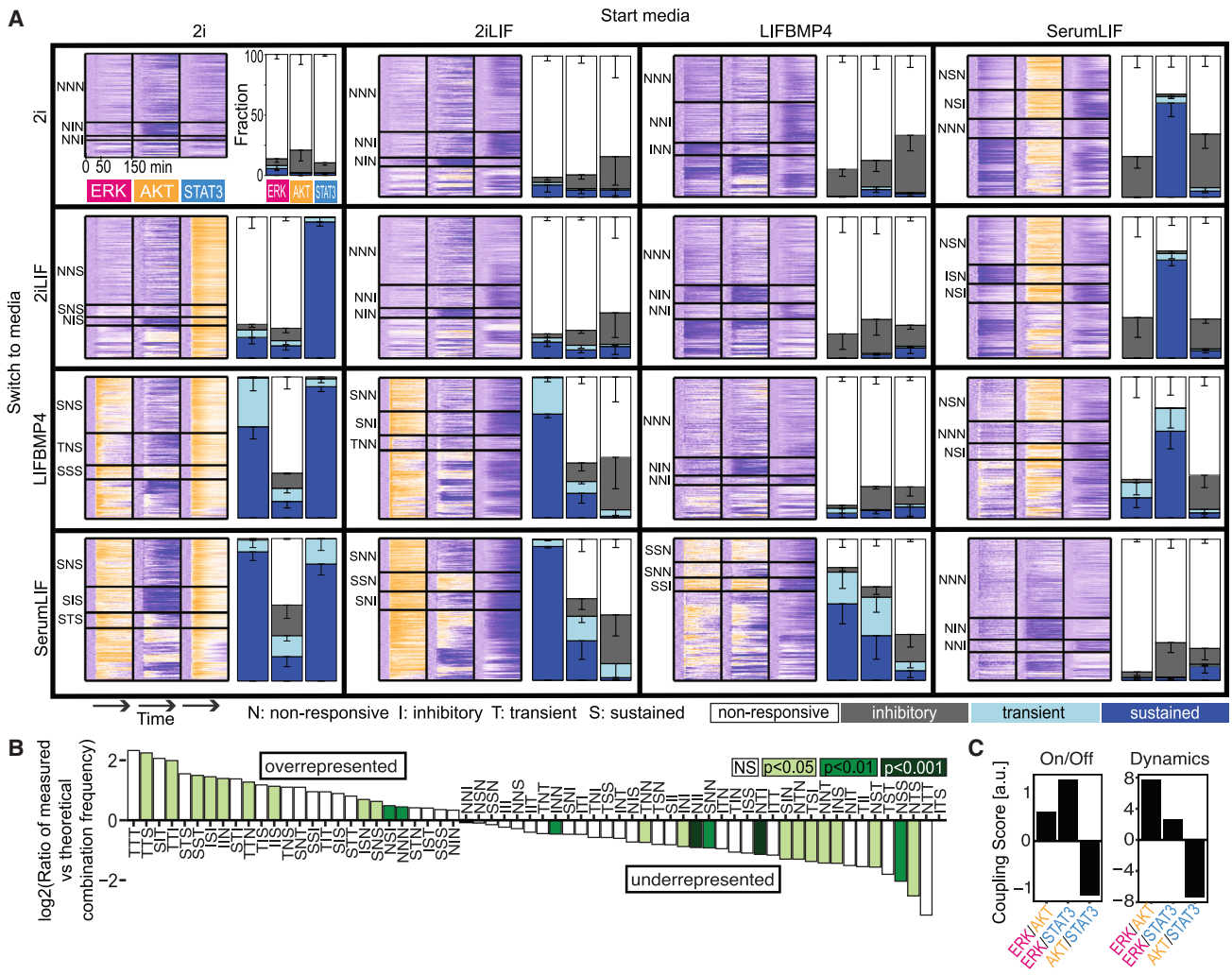

Figure 3. ERK, AKT, and STAT3 dynamics are largely independent and can occur in almost any theoretically possible combination

(A) Heat maps: simultaneous single ESC dynamics for all three pathways. Pathways are measured separately and simultaneously in individual cells. Signaling dynamics of many individual cells are shown as stacked heat stripes (compare Figure 1C for a single cell). Heat stripes for the three pathways are shown in one line representing one cell for clustering. Some switch conditions have one or a few dominant dynamics combinations, but often many combinations occur, suggesting independence of signaling pathways. The three most abundant combinations for each condition are labeled (N = NON, T = TRA, S = SUS, I = INH). Bar graphs represent fractions of signaling behavior for all pathways in all conditions. Signaling dynamics are highly heterogeneous, both between individual ESCs and between media conditions. Error bars represent SD. N = 3 independent samples (cell populations), n > 500 cells per condition.

(B) Ratios between measured fractions of a specific pathway dynamics combination and its theoretical fraction based on the abundance of the dynamics of the individual pathways. A high ratio means that the dynamics combination was measured more often than it is expected based on the single pathway dynamics. Several combinations are significantly over- or underrepresented, which suggests reciprocal influence between the pathways or joined regulation by shared upstream effectors. Green = statistically significant (light = $p < 0.05$, medium = $p < 0.01$, dark = $p < 0.001$).

(C) Coupling scores indicating strength of correlation between the dynamics of two pathways. On/Off: only activation vs. no activation is considered. Dynamics: all behaviors (NON, INH, TRA, SUS) are considered. ERK and AKT often respond similarly to the same stimuli, whereas AKT and STAT3 rarely do. See supplemental methods for details about calculation. N = 3 independent samples (cell populations) measured in 12 independent experiments. See also Figure S3.

the media condition, demonstrating minimal baseline fluctuations due to technical and biological noise (Figure 3A). As expected, dynamics were partly dependent on the pathway activity before the medium switch, with already active cells on average responding less strongly or even with decreasing signaling levels (Figure S3D). However,

the number of cells with a baseline activity that did not allow for further activation (Figure S3D, magenta threshold line) was very low (Figure S3E). The vast majority of cells showed a baseline activity that allowed for all four dynamics types. Thus, baseline activity does not predict signaling dynamics or cell behavior.

We next quantified their single-cell pathway dynamics combinations (Figures 3A, S3A, and S3B). This was possible only due to our simultaneous multiplexed single-cell dynamics analysis of three pathways. With three pathways and four possible dynamics, 64 combinations are theoretically possible. Of the conditions with a real medium switch (Figure 3A, non-diagonal panels), only the switch from 2iLIF to 2i showed a dominant combination with >50% of cells not responding in all three pathways. In all other switch conditions, even the most common combination was present in <50% of cells, with multiple larger fractions of different combinations (Figure 3A). For example, after the switch from LIFBMP4 to SerumLIF, even the most abundant $ERK^{SUS}AKT^{SUS}STAT3^{NON}$ combination was present in only 17% of ESCs. 11% showed $ERK^{SUS}AKT^{NON}STAT3^{NON}$, 10% $ERK^{SUS}AKT^{SUS}STAT3^{INH}$, and even fewer ESCs one of the many other combinations. This illustrates the vast heterogeneity between ESCs even when cultured in the same conditions and responding to the same stimulus.

We analyzed if specific dynamics combinations are more or less likely to co-occur, i.e., if they are over- or underrepresented compared with others. To this end, we combined the data from all conditions and determined the theoretical abundance of each of the 64 different combinations based on the quantified dynamics frequencies of individual pathways. For instance, 25%, 24%, and 21% of all ESCs show SUS dynamics in ERK, AKT, and STAT3, respectively. If pathways were fully independent, the expected random frequency of this $ERK^{SUS}AKT^{SUS}STAT3^{SUS}$ combination would be 25% × 24% x 21% = 1.26%. However, many of the measured combinations were considerably under- or over-represented relative to the theoretical independent expectation (Figure 3B). This suggests their co-/anti-regulation due to crosstalk between pathways or common responses to shared upstream effectors. To quantify the pairwise relationship between pathways, we calculated a coupling score as the product of the over/under representation values of all combinations with the same activation or with the same dynamics in the two pathways (Figure 3C; see supplemental methods for details). If only activation vs. no activation (i.e., On/Off) of each pathway is considered, ERK and STAT3 are most strongly associated with each other (Figure 3C, left). Interestingly, when the different dynamics are distinguished, ERK and AKT dynamics are strongly correlated, while ERK and STAT3 are more independent (Figure 3C, right). Combinations where AKT and STAT3 show the same dynamics are considerably underrepresented, suggesting an opposing role for these pathways in ESCs. However, even though the pathways influence each other and are partly (anti-) correlated, it is important to note that 63 of the 64 possible combinations were detected. This shows that ERK, AKT, and STAT3 responses can be independent, and activity of one pathway does not necessarily determine the response of another one. This is surprising, considering the wiring and interconnectivity of these pathways that would suggest a more correlated behavior. Taken together, these data underline the great extent of signaling heterogeneity from cell to cell and suggest existing but context-dependent links between the measured pathways.

Cell cycle influences total NANOG content and ERK dynamics in ESCs

To evaluate potential sources and relevance of the observed signaling heterogeneity, we investigated the relationship of non-signaling related ESC properties with the measured dynamics. To this end, we imaged ESCs for an entire cell cycle (CC), and in addition to signaling activity of ERK and STAT3, we quantified several morphological properties and cellular NANOG protein content as a metric of pluripotency (Hastreiter and Schroeder, 2016). The novel cell line for this experiment was created by stable integration of an ERKmRuby2/STAT3mCerulean3 double-reporter construct (plus an iRFPnucmem marker for nuclear segmentation) into an R1 NANOGVENUS ESC line (Filipczyk et al., 2013, 2015). With this resulting "NVERSC" ESC line, we utilize four orthogonal fluorescence colors to simultaneously quantify live signaling dynamics of ERK and STAT3 plus NANOG levels that serve as a proxy for their pluripotency versus differentiation state. To capture full CCs of quantified ESCs, they were imaged every 30 min for a total of 2 days. After 10–14 h, medium was switched from 2i to LIFBMP4. From 30 min before to 60 min after medium switch, signaling dynamics were imaged with high frequency (5 min interval) (Figure S4E) to capture fast signaling dynamics. Cells that underwent division in the 10–14 h before stimulation were identified retrospectively and selected for further analysis. Since single ESCs were in different states of the CC at the time of stimulation, we could evaluate the fractions of SUS and TRA responders depending on CC progression. Absolute CC length was normalized to 1 for each cell, and fractional progression along the CC was analyzed as a proxy for CC progression. Interestingly, ESCs early in the cycle exhibited ERK^{SUS} dynamics more frequently than ESCs in a later CC state (Figure 4A). Thus, CC could be an undervalued source of heterogeneity and explains some of the observed single-cell variations, as also described *in vivo* (Pokrass et al., 2020). In contrast, CC state had no significant influence on STAT3 signaling (Figure 4A).

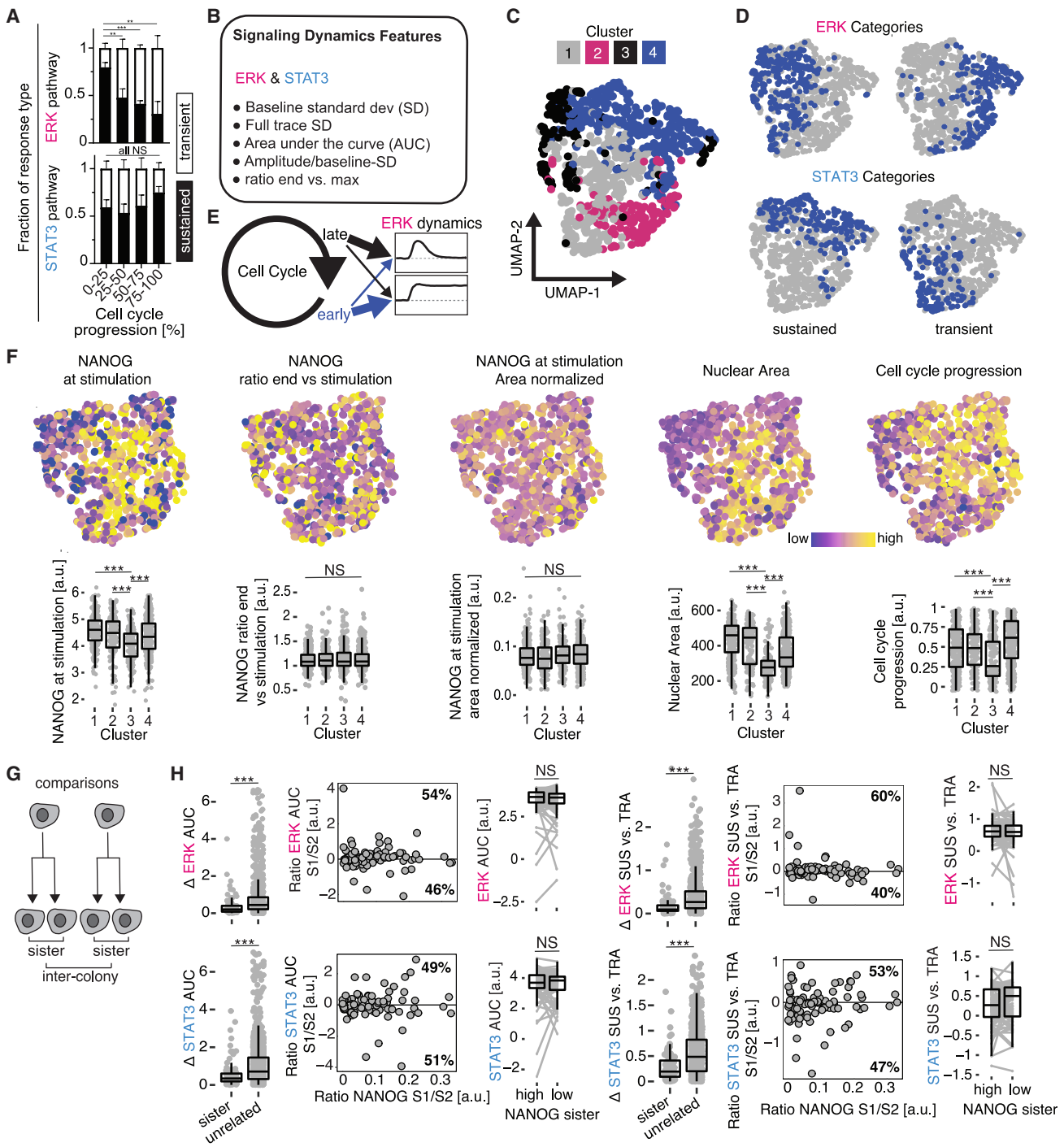

Figure 4. Cell cycle state and NANOG levels correlate and partly predict dynamical signaling behavior

(A) Response dynamics depending on the cell cycle stage. For ERK, but not STAT3, CC progression increases TRA at the expense of SUS dynamics. ESCs were observed through their entire lifetime from the mother ESC until their own division. Lifetime/cell cycle was binned into four groups of equal relative duration. Error bars = SD.

(B) Single-cell signaling features based on ERK and STAT3 dynamics. Extracted features can be used to cluster ESCs in a signaling dynamics "landscape."

(legend continued on next page)

We complemented our previous, threshold-based analysis by extracting 10 distinct features of both ERK and STAT3 signaling time series and calculating scores for each feature and single cell (Figure 4B). ESCs were categorized by hierarchical clustering of feature scores, visualized by uniform manifold approximation and projection (UMAP) (Figure 4C). Projection of the previously assigned, threshold-based classes onto the UMAP shows almost no overlap between SUS and TRA ESCs (Figure 4D). Thus, feature and threshold-based classification methods confirm each other. We next analyzed the correlation of several non-signaling-related features with signaling feature space clusters (Figure 4F). Importantly, these features are independent and did not contribute to the UMAP or cluster generation. Interestingly, we observed a correlation of low NANOG levels with signaling cluster 3. However, the differences disappeared when NANOG levels were normalized to nuclear area, suggesting that cell size or adhesion/shape rather than pluripotency predicts signaling behavior. CC progression also differed between clusters, potentially explaining part of the signaling-area correlation, since CC and area are strongly correlated.

The observed CC phase dependency suggests that signaling dynamics states could change very rapidly, within minutes or hours. Alternatively, uneven exposure to micro-environmental stimuli, e.g., due to different locations of the ESCs within a culture device or colony, could be an external source of inter-cellular signaling variation. To control for CC variability and differences of external influences, we imaged single ESCs in 2i media for 12 h and subsequently stimulated them with LIFBMP4 while observing their signaling dynamics (Figure S4F). We retrospectively identified cells that divided once or twice before stimulation and performed a comparison of paired sister cell differences. This comparison removes both environmental and inter-clonal variability and thus enables a much cleaner evaluation of the relationship between cell-intrinsic properties and signaling behavior (Figure 4G). Interestingly, in all analyzed features (signaling and non-signaling), sister ESCs were much more similar to each other than to non-related ESCs (Figure 4H, left panels). This confirms that the previously described cell-to-cell heterogeneity is not an artifact of technical noise but caused by cell-intrinsic properties. When ESCs of sister pairs were sorted according to their NANOG levels, we did not find a significant difference in signaling behavior between NANOG low and high sisters (Figure 4H, right panels). Supporting our findings above and in contrast to a previous study (Kale et al., 2022), this suggests that pluripotency and ERK/STAT3 dynamics are indeed independent.

DISCUSSION

In this study, we accomplish the first simultaneous quantification of the activity dynamics of ERK, AKT, and STAT3 signaling in live single mouse ESCs. This confirmed previous, snapshot-based results that LIF highly activates STAT3 and ERK and the strongly activating and inhibiting influence of serum and 2i on ERK signaling, respectively (Niwa et al., 2009; Ying et al., 2003, 2008). These findings thus corroborate the functionality and sensitivity of our experimental setup and quantification approach. Our results contradict earlier studies that claimed activation of AKT by LIF. Supposedly, LIF activates PI3K/AKT by JAKs-dependent phosphorylation leading to increased self-renewal capacity (Hirai et al., 2011; Paling et al., 2004). 2i was the only of our media conditions not containing LIF. After switching from 2i to any of the three LIF-containing media, we could observe AKT activation only in very few cells but never throughout the population. In addition, withdrawal of LIF did not seem to have an influence on AKT activity. A possible influence of LIF on AKT could be masked by other components such as 2i, BMP4, or Serum in our pluripotency media. However, previous conclusions on the activation of PI3K/AKT by LIF activated JAKs were

(C) Several signaling dynamics clusters can be distinguished by hierarchical clustering. The number of clusters was chosen based on separation quality. The clusters separate well in the two-dimensional uniform manifold approximation and projection (UMAP) representation of the higher dimensional landscape.
(D) Localization of threshold-based dynamics classes within the feature-based UMAP. Good separation of TRA and SUS dynamics for ERK and STAT3 show that feature-based dynamics classification confirms threshold-based classification.
(E) Summary of CC influence on ERK signaling dynamics.
(F) Mapping of non-signaling-related properties onto the signaling dynamics landscape. NANOG levels, nuclear area, and CC progression differ between clusters and therefore seem to be dynamics dependent. The difference in NANOG levels disappears if it is normalized by the nuclear area (which correlates with CC). N = 2 independent samples (cell populations), n = 949 cells. p-values from two sided t tests.
(G) Comparison of sister ESCs reduces CC and environmentally induced variability.
(H) Left: signaling dynamics and non-signaling-related properties are more similar between sister ESCs than unrelated ESCs. S1/2 = sister1/2. N = 2 independent samples (cell populations) measured in two independent experiments, with 84 individual sister pairs. Middle and right: ERK and STAT3 signaling activity depending on NANOG expression. NANOG expression does not predict ERK or STAT3 dynamics or activity. Sister cells within a pair are sorted according to their NANOG levels (S1 > S2). See also Figure S4.

only inferred but not measured in ESCs and might have been due to only a correlation of LIF and AKT (caused by, e.g., crosstalk between MEK/ERK and PI3K/AKT) rather than direct activation. This weak link between LIF and AKT—causative or correlative—is likely condition dependent and does not show up in our data. It is interesting to note that all tested media conditions support pluripotency, but they trigger quite different signaling cascades, confirming that pluripotency is not a property that can be achieved by only one specific external (niche) influence and signaling activity.

In contrast to previous studies, we quantify three pathways simultaneously in single ESCs and are therefore able to correlate the individual pathways with each other in dependence of culture condition. ERK and AKT are correlated in many cases. However, individual cells often show a different behavior, opposing the signaling dynamics of the entire population. This shows that dynamics of one pathway are not necessarily determined by another pathway or specific stimuli, but instead, they are (also) dependent on the state of the individual ESC. Since ERK and AKT are opposing each other in terms of pluripotency maintenance (Watanabe et al., 2006), the simultaneous measurement of both pathways now also allows for the identification of cell populations that maintain ($ERK^{down/low}AKT^{up}$) or exit ($ERK^{up}AKT^{down/low}$) pluripotency as well as intermediate states. Rare cell populations with specific behaviors are missed when analyzing low cell numbers (Deathridge et al., 2019; Simon et al., 2020), showing the necessity of quantifying many (here >10,000) single cells for robust conclusions. Even though ESCs are known to be heterogeneous and were described to switch between different states in culture (Chakraborty et al., 2020), the vast cell-to-cell variation in signaling dynamics was surprising. The fact that sister ESCs behave much more similarly to each other than to unrelated ESCs excludes technical noise as a source of variation and demonstrates cell-intrinsic memory.

CC state and NANOG levels were obvious candidates for sources of heterogeneity, since variations in NANOG levels in ESCs had been extensively studied in the past (Hastreiter et al., 2018). CC state at stimulation partly explains ERK signaling heterogeneity. However, further investigations are needed to find additional sources of heterogeneity and to explain variations in other pathways. Interestingly, weak correlations between NANOG levels and signaling dynamics that we initially discovered can be explained by the CC-state-dependent different NANOG content of ESCs. We confirmed these findings by analysis of sister cells that are naturally synchronized in CC and experience very similar environmental stimuli because of their physical proximity. There was no significant relationship between NANOG levels and signaling in CC-synchronized sister cell assays. Taken together, this suggests that signaling behavior is insensitive toward small changes in pluripotency and might change only in strict differentiation conditions. This could potentially be a mechanism of ESCs to filter noise, retain pluripotency upon spurious stimulation by transient inputs from the environment, and avoid premature differentiation. Overall, this shows that, despite their central role in regulating pluripotency, ERK and STAT3 signaling dynamics are insensitive to underlying variations in NANOG levels. It is therefore unlikely that they are affected by early differentiation events.

Our approach to measure single-cell dynamics of multiple signaling pathways can now be applied also to other pathway combinations and cell systems. It will be enlightening to further investigate the implications of signaling heterogeneity for cellular fate (Ryu et al., 2015) in ESCs and other stem cells and potentially enforce certain fate decisions by precisely controlling signaling. This could be enabled by optogenetic tools (Dessauges et al., 2021; Toettcher et al., 2013) that are just getting established for these pathways or fluidics manipulation (Dettinger et al., 2022). Enforcing specific signaling dynamics without altering other cellular properties and subsequent analysis of ESC behavior will be ideal to test for causal links between signaling dynamics, molecular target programs (Wehling et al., 2022), and fate control (Kull et al., 2022). Precise signaling manipulation will then also allow for a new degree of control in *in vitro* culture systems and potentially lead to major advances in stem cell expansion, differentiation protocols, and disease modeling.

EXPERIMENTAL PROCEDURES

Resource availability

Corresponding author

Further information and requests for resources and reagents should be directed to and will be fulfilled by the lead contact, Timm Schroeder (timm.schroeder@bsse.ethz.ch).

Materials availability

Cell lines and plasmids will be available from the lead contact upon reasonable request.

Data and code availability

Analysis scripts and complementary data used in this publication can be found in the supplemental information.

Experimental model and subject details

Ethical statement

All experiments were done according to Swiss federal law and institutional guidelines of ETH Zurich.

Parental mESC lines

R1 WT cells (male) were obtained from Konstantinos Anastassiadis at the Transgenic Core Facility of the Technical University of

Dresden, and R1 NANOGVENUS is published (Filipczyk et al., 2013). The cell lines were negatively tested for mycoplasma.

Cell culture

Cell lines were maintained on 0.1% porcine gelatin-coated tissue culture dishes in DMEM supplemented with 10% FCS, 10 ng/mL LIF, 2 mM GlutaMAX, 1% non-essential amino acids, 1 mM sodium pyruvate, and 50 μM β-mercaptoethanol at 37°C and 5% CO_2. Every second day, cells were passaged with 0.25% trypsin-EDTA to a density of 1,000 cells/cm^2. For details about culture during time-lapse movies, see supplemental methods.

Proliferation assay

Cell lines were cultured in SerumLIF and passaged every 48 h on gelatin solution at 20,000 cells/cm^2 for 14 days in duplicates in separate wells.

Cloning

See supplemental methods.

Generation of stable cell lines

R1 WT or R1 NANOGVENUS parental cell lines were seeded at 2 x 10^4 cells/cm^2 in standard culture conditions. 1 day later, 2.1 μg DNA (1,500 ng transposon plasmid containing the expression cassette and 600 ng transposase plasmid) were transfected with 4 μL lipofectamine 2000 in a total volume of 100 μL Opti-MEM. 7 days later, cells positive for all fluorescent markers were sorted using a FACS ARIA III (BD Biosciences) either in bulk for polyclonal lines or as single cells in a 384-well plate for monoclonal lines.

Flow cytometry analysis

Poly- or monoclonal cell lines were analyzed for the presence of expression markers 5 weeks after sorting with a BD LSR Fortessa (BD Biosciences). 20,000 cells were analyzed per cell line.

Neuroectoderm differentiation assay

1,200 cells/cm^2 in an Ibidi 96-well plate were seeded on StemAdhere in neuroectoderm differentiation medium NDiff 227+ retinoic acid (1:20,000). 2.5 days later, cells were fixed and analyzed for expression of neuroectoderm marker SOX1 using immunostainings.

Immunostaining

See supplemental methods.

Time-lapse microscopy

Image acquisition was performed on Nikon Ti-E microscope with a Nikon 10x Plan Fluor objective, Nikon Perfect Focus Systems, Lumencor Spectra X light engine, and Hamamatsu Orca Flash 4.0 V2 camera. The microscope was surrounded by a home-built box, and temperature was controlled by The Cube from LIFe Imaging Services. For details about laser and filter settings, see supplemental methods.

Image processing, tracking, and quantification

16-bit to 8-bit conversion (to reduce file sizes) was applied to the image series (consisting of .png files) using an in-house developed software and corrected for background shading artifacts in images and over time (Peng et al., 2017). IRFPnucmem-expressing nuclei were segmented using FastER (Hilsenbeck et al., 2017) and tracked over time either automatically (Magnusson et al., 2015) or manually (Hilsenbeck et al., 2016). Visual inspection and correction of tracked cells were done in tTt and quantification in qTfy (Hilsenbeck et al., 2016). In the rare cases where an ESC died before the end of the movie, it was excluded from the dataset. In the short 2.5-h movies that quantify signaling behavior for different medium switches (Figures 1, 2, and 3), we excluded the rare cells that divided during imaging and would thus have too short observation periods.

Further processing steps of quantified signaling traces

See supplemental methods.

Threshold-based time series classification

See supplemental methods.

Feature-based time series analysis

Five features for each ERK and STAT3 signaling curves were defined, and single scores for each feature were calculated per cell. Distribution of cells within the 10-dimensional feature space was evaluated by using the non-linear dimensionality reduction method UMAP (umap() function in R 3.4.2). For details about features, their calculation, and meaning, please refer to the deposited R-script 220304_ESC_dynamics_analysis.R.

Quantification and statistical analysis

All quantification and statistical analyses were done in the programming environment R (R 3.4.2, R-Project). Details of statistical analyses are indicated in the legends of the respective figures. If not indicated otherwise, it was assumed that the data were distributed normally, and a standard two-sided t test was performed. Statistical significance was defined as follows: *$p < 0.05$; **$p < 0.01$; ***$p < 0.001$. No statistical methods were used to predetermine sample size. Experiments were not randomized, and investigators were not blinded to allocation during experiments and outcome assessment.

Data and materials availability

Videos S1, S2, S3, S4, S5, S6, S7, S8, and S9 and Datasets S1, S2, S3, and S4 can found in the supplemental information.

SUPPLEMENTAL INFORMATION

Supplemental information can be found online at https://doi.org/10.1016/j.stemcr.2023.04.008.

AUTHOR CONTRIBUTIONS

Conceptualization, T.S., A.R., and T.K.; methodology, A.R. and T.K.; investigation, A.R., T.K., W.W., and P.D.; data curation, A.R. and T.K.; formal analysis, A.R. and T.K.; software, T.K., T.S., A.R., and D.L.; visualization, A.R., T.K., and T.S.; supervision, T.S.; resources, T.S. and D.L.; writing – original draft, T.K. and T.S.; writing – review & editing, T.S., A.R., W.W., P.D., and D.L.; project administration, T.S.; funding acquisition, T.S.

ACKNOWLEDGMENTS

We thank V. Jäggin, T. Lopes, T. Lummen, and E. Montani for technical support. This work was supported by Swiss National Science Foundation grant 179490 and a "Personalized Medicine Basel" grant to T.S.

CONFLICT OF INTERESTS

The authors declare no competing interests.

Received: August 16, 2022
Revised: April 17, 2023
Accepted: April 18, 2023
Published: May 18, 2023

REFERENCES

Ahmed, N., Etzrodt, M., Dettinger, P., Kull, T., Loeffler, D., Hoppe, P.S., Chavez, J.S., Zhang, Y., Camargo Ortega, G., Hilsenbeck, O., et al. (2022). Blood stem cell PU.1 upregulation is a consequence of differentiation without fast autoregulation. J. Exp. Med. *219*, e20202490.

Chakraborty, M., Hu, S., Visness, E., Del Giudice, M., Garg, S., De Martino, A., Bosia, C., Sharp, P.A., and Garg, S. (2020). MicroRNAs organize intrinsic variation into stem cell states. Proc. Natl. Acad. Sci. USA *117*, 6942–6950.

Chambers, I., Colby, D., Robertson, M., Nichols, J., Lee, S., Tweedie, S., and Smith, A. (2003). Functional expression cloning of Nanog, a pluripotency sustaining factor in embryonic stem cells. Cell *113*, 643–655.

Chambers, I., Silva, J., Colby, D., Nichols, J., Nijmeijer, B., Robertson, M., Vrana, J., Jones, K., Grotewold, L., and Smith, A. (2007). Nanog safeguards pluripotency and mediates germline development. Nature *450*, 1230–1234.

Chen, H., Guo, R., Zhang, Q., Guo, H., Yang, M., Wu, Z., Gao, S., Liu, L., and Chen, L. (2015). Erk signaling is indispensable for genomic stability and self-renewal of mouse embryonic stem cells. Proc. Natl. Acad. Sci. USA *112*, E5936–E5943.

Deathridge, J., Antolović, V., Parsons, M., and Chubb, J.R. (2019). Live imaging of erk signalling dynamics in differentiating mouse embryonic stem cells. Development *146*, dev172940.

Dessauges, C., Mikelson, J., Dobrzynski, M., Jacques, M.-A., Frismantiene, A., Gagliardi, P.A., Khammash, M., and Pertz, O. (2021). Optogenetic actuator/biosensor circuits for large-scale interrogation of ERK dynamics identify sources of MAPK signaling robustness. Preprint at bioRxiv. https://doi.org/10.1101/2021.07.27.453955.

Dettinger, P., Kull, T., Arekatla, G., Ahmed, N., Zhang, Y., Schneiter, F., Wehling, A., Schirmacher, D., Kawamura, S., Loeffler, D., et al. (2022). Open-source personal pipetting robots with live-cell incubation and microscopy compatibility. Nat. Commun. *13*, 2999.

Eilken, H.M., Nishikawa, S.-I., and Schroeder, T. (2009). Continuous single-cell imaging of blood generation from haemogenic endothelium. Nature *457*, 896–900.

Endele, M., and Schroeder, T. (2012). Molecular live cell bioimaging in stem cell research. Ann. N. Y. Acad. Sci. *1266*, 18–27.

Etzrodt, M., Endele, M., and Schroeder, T. (2014). Quantitative single-cell approaches to stem cell research. Cell Stem Cell *15*, 546–558.

Filipczyk, A., Gkatzis, K., Fu, J., Hoppe, P.S., Lickert, H., Anastassiadis, K., and Schroeder, T. (2013). Biallelic expression of nanog protein in mouse embryonic stem cells. Cell Stem Cell *13*, 12–13.

Filipczyk, A., Marr, C., Hastreiter, S., Feigelman, J., Schwarzfischer, M., Hoppe, P.S., Loeffler, D., Kokkaliaris, K.D., Endele, M., Schauberger, B., et al. (2015). Network plasticity of pluripotency transcription factors in embryonic stem cells. Nat. Cell Biol. *17*, 1235–1246.

Filonov, G.S., Piatkevich, K.D., Ting, L.M., Zhang, J., Kim, K., and Verkhusha, V.V. (2011). Bright and stable near-infrared fluorescent protein for in vivo imaging. Nat. Biotechnol. *29*, 757–761.

Graf, T., and Stadtfeld, M. (2008). Heterogeneity of embryonic and adult stem cells. Cell Stem Cell *3*, 480–483.

Gross, S.M., and Rotwein, P. (2015). Akt signaling dynamics in individual cells. J. Cell Sci. *128*, 2509–2519.

Hastreiter, S., and Schroeder, T. (2016). Nanog dynamics in single embryonic stem cells. Cell Cycle *15*, 770–771.

Hastreiter, S., Skylaki, S., Loeffler, D., Reimann, A., Hilsenbeck, O., Hoppe, P.S., Coutu, D.L., Kokkaliaris, K.D., Schwarzfischer, M., Anastassiadis, K., et al. (2018). Inductive and selective effects of GSK3 and MEK inhibition on nanog heterogeneity in embryonic stem cells. Stem Cell Rep. *11*, 58–69.

Herrmann, A., Sommer, U., Pranada, A.L., Giese, B., Küster, A., Haan, S., Becker, W., Heinrich, P.C., and Müller-Newen, G. (2004). STAT3 is enriched in nuclear bodies. J. Cell Sci. *117*, 339–349.

Hilsenbeck, O., Schwarzfischer, M., Skylaki, S., Schauberger, B., Hoppe, P.S., Loeffler, D., Kokkaliaris, K.D., Hastreiter, S., Skylaki, E., Filipczyk, A., et al. (2016). Software tools for single-cell tracking and quantification of cellular and molecular properties. Nat. Biotechnol. *34*, 703–706.

Hilsenbeck, O., Schwarzfischer, M., Loeffler, D., Dimopoulos, S., Hastreiter, S., Marr, C., Theis, F.J., and Schroeder, T. (2017). fastER: a user-friendly tool for ultrafast and robust cell segmentation in large-scale microscopy. Bioinformatics *33*, 2020–2028.

Hirai, H., Karian, P., and Kikyo, N. (2011). Regulation of embryonic stem cell self-renewal and pluripotency by leukaemia inhibitory factor. Biochem. J. *438*, 11–23.

Hoppe, P.S., Coutu, D.L., and Schroeder, T. (2014). Single-cell technologies sharpen up mammalian stem cell research. Nat. Cell Biol. *16*, 919–927.

Hoppe, P.S., Schwarzfischer, M., Loeffler, D., Kokkaliaris, K.D., Hilsenbeck, O., Moritz, N., Endele, M., Filipczyk, A., Gambardella, A., Ahmed, N., et al. (2016). Early myeloid lineage choice is not initiated by random PU.1 to GATA1 protein ratios. Nature *535*, 299–302.

Kale, H.T., Rajpurohit, R.S., Jana, D., Vishnu, V.V., Srivastava, M., Mourya, P.R., Srinivas, G., and Shekar, P.C. (2022). A NANOG-pERK reciprocal regulatory circuit regulates Nanog autoregulation and ERK signaling dynamics. EMBO Rep. *23*, e54421.

Kim, M.O., Kim, S.H., Cho, Y.Y., Nadas, J., Jeong, C.H., Yao, K., Kim, D.J., Yu, D.H., Keum, Y.S., Lee, K.Y., et al. (2012). ERK1 and ERK2 regulate embryonic stem cell self-renewal through phosphorylation of Klf4. Nat. Struct. Mol. Biol. *19*, 283–290.

Klein, A.M., Mazutis, L., Akartuna, I., Tallapragada, N., Veres, A., Li, V., Peshkin, L., Weitz, D.A., and Kirschner, M.W. (2015). Droplet barcoding for single-cell transcriptomics applied to embryonic stem cells. Cell *161*, 1187–1201.

Kull, T., and Schroeder, T. (2021). Analyzing signaling activity and function in hematopoietic cells. J. Exp. Med. *218*, e20201546.

Kull, T., Wehling, A., Etzrodt, M., Auler, M., Dettinger, P., Aceto, N., and Schroeder, T. (2022). NfκB signaling dynamics and their target genes differ between mouse blood cell types and induce distinct cell behavior. Blood *140*, 99–111.

Lane, K., Van Valen, D., DeFelice, M.M., Macklin, D.N., Kudo, T., Jaimovich, A., Carr, A., Meyer, T., Pe'er, D., Boutet, S.C., et al. (2017). Measuring signaling and RNA-seq in the same cell links gene expression to dynamic patterns of NF-κB activation. Cell Syst. *4*, 458–469.e5.

Li, Z., Fei, T., Zhang, J., Zhu, G., Wang, L., Lu, D., Chi, X., Teng, Y., Hou, N., Yang, X., et al. (2012). BMP4 signaling acts via dual-specificity phosphatase 9 to control ERK activity in mouse embryonic stem cells. Cell Stem Cell *10*, 171–182.

Loeffler, D., Wehling, A., Schneiter, F., Zhang, Y., Müller-Bötticher, N., Hoppe, P.S., Hilsenbeck, O., Kokkaliaris, K.D., Endele, M., and Schroeder, T. (2019). Asymmetric lysosome inheritance predicts activation of haematopoietic stem cells. Nature *573*, 426–429.

Loeffler, D., Schneiter, F., Wang, W., Wehling, A., Kull, T., Lengerke, C., Manz, M.G., and Schroeder, T. (2021). Asymmetric organelle inheritance predicts human blood stem cell fate. Blood *139*, 2011–2023.

Lorusso, P.M., Adjei, A.A., Varterasian, M., Gadgeel, S., Reid, J., Mitchell, D.Y., Hanson, L., DeLuca, P., Bruzek, L., Piens, J., et al. (2005). A phase 1–2 clinical study of a second generation oral MEK inhibitor, PD 0325901 in patients with advanced cancer. J. Clin. Oncol. *23*, 5281–5293.

Magnusson, K.E.G., Jalden, J., Gilbert, P.M., and Blau, H.M. (2015). Global linking of cell tracks using the viterbi algorithm. IEEE Trans. Med. Imaging *34*, 911–929.

Marks, H., Kalkan, T., Menafra, R., Denissov, S., Jones, K., Hofemeister, H., Nichols, J., Kranz, A., Stewart, A.F., Smith, A., et al. (2012). The transcriptional and epigenomic foundations of ground state pluripotency. Cell *149*, 590–604.

Marshall, C.J. (1995). Specificity of receptor tyrosine kinase signaling: transient versus sustained extracellular signal-regulated kinase activation. Cell *80*, 179–185.

Ng, H.H., and Surani, M.A. (2011). The transcriptional and signalling networks of pluripotency. Nat. Cell Biol. *13*, 490–496.

Niwa, H., Ogawa, K., Shimosato, D., and Adachi, K. (2009). A parallel circuit of LIF signalling pathways maintains pluripotency of mouse ES cells. Nature *460*, 118–122.

Okita, C., Sato, M., and Schroeder, T. (2004). Generation of optimized yellow and red fluorescent proteins with distinct subcellular localization. Biotechniques *36*, 418–422.

Paling, N.R.D., Wheadon, H., Bone, H.K., and Welham, M.J. (2004). Regulation of embryonic stem cell self-renewal by phosphoinositide 3-kinase-dependent signaling. J. Biol. Chem. *279*, 48063–48070.

Peng, T., Thorn, K., Schroeder, T., Wang, L., Theis, F.J., Marr, C., and Navab, N. (2017). A BaSiC tool for background and shading correction of optical microscopy images. Nat. Commun. *8*, 14836.

Pokrass, M.J., Ryan, K.A., Xin, T., Pielstick, B., Timp, W., Greco, V., and Regot, S. (2020). Cell-cycle-dependent ERK signaling dynamics direct fate specification in the mammalian preimplantation embryo. Dev. Cell *55*, 328–340.e5.

Purvis, J.E., Karhohs, K.W., Mock, C., Batchelor, E., Loewer, A., and Lahav, G. (2012). p53 dynamics control cell fate. Science *336*, 1440–1444.

Raina, D., Fabris, F., Morelli, L.G., and Schröter, C. (2022). Intermittent ERK oscillations downstream of FGF in mouse embryonic stem cells. Development *149*, dev199710.

Regot, S., Hughey, J.J., Bajar, B.T., Carrasco, S., and Covert, M.W. (2014). High-sensitivity measurements of multiple kinase activities in live single cells. Cell *157*, 1724–1734.

Rieger, M.A., Hoppe, P.S., Smejkal, B.M., Eitelhuber, A.C., and Schroeder, T. (2009). Hematopoietic cytokines can instruct lineage choice. Science *325*, 217–218.

Ryu, H., Chung, M., Dobrzyński, M., Fey, D., Blum, Y., Lee, S.S., Peter, M., Kholodenko, B.N., Jeon, N.L., and Pertz, O. (2015). Frequency modulation of ERK activation dynamics rewires cell fate. Mol. Syst. Biol. *11*, 838.

Schroeder, T. (2005). Tracking hematopoiesis at the single cell level. Ann. N. Y. Acad. Sci. *1044*, 201–209.

Schulz, E.G., Meisig, J., Nakamura, T., Okamoto, I., Sieber, A., Picard, C., Borensztein, M., Saitou, M., Blüthgen, N., and Heard, E. (2014). The two active X chromosomes in female ESCs block exit from the pluripotent state by modulating the ESC signaling network. Cell Stem Cell *14*, 203–216.

Simon, C.S., Rahman, S., Raina, D., Schröter, C., and Hadjantonakis, A.K. (2020). Live visualization of ERK activity in the mouse blastocyst reveals lineage-specific signaling dynamics. Dev. Cell *55*, 341–353.e5.

Singh, D.K., Ku, C.J., Wichaidit, C., Steininger, R.J., Wu, L.F., and Altschuler, S.J. (2010). Patterns of basal signaling heterogeneity can distinguish cellular populations with different drug sensitivities. Mol. Syst. Biol. *6*, 369.

Smith, A.G., Heath, J.K., Donaldson, D.D., Wong, G.G., Moreau, J., Stahl, M., and Rogers, D. (1988). Inhibition of pluripotential embryonic stem cell differentiation by purified polypeptides. Nature *336*, 688–690.

Tay, S., Hughey, J.J., Lee, T.K., Lipniacki, T., Quake, S.R., and Covert, M.W. (2010). Single-cell NF-κB dynamics reveal digital activation and analogue information processing. Nature *466*, 267–271.

Toettcher, J.E., Weiner, O.D., and Lim, W.A. (2013). Using optogenetics to interrogate the dynamic control of signal transmission by the Ras/Erk module. Cell *155*, 1422–1434.

Torres-Padilla, M.E., and Chambers, I. (2014). Transcription factor heterogeneity in pluripotent stem cells: a stochastic advantage. Development *141*, 2173–2181.

Wang, W., Zhang, Y., Dettinger, P., Reimann, A., Kull, T., Loeffler, D., Manz, M.G., Lengerke, C., and Schroeder, T. (2021). Cytokine combinations for human blood stem cell expansion induce cell type- and cytokine-specific signaling dynamics. Blood *138*, 847–857.

Watanabe, S., Umehara, H., Murayama, K., Okabe, M., Kimura, T., and Nakano, T. (2006). Activation of Akt signaling is sufficient to maintain pluripotency in mouse and primate embryonic stem cells. Oncogene *25*, 2697–2707.

Wehling, A., Loeffler, D., Zhang, Y., Kull, T., Donato, C., Szczerba, B., Camargo Ortega, G., Lee, M., Moor, A., Göttgens, B., et al. (2022). Combining single-cell tracking and omics improves blood stem cell fate regulator identification. Blood *140*, 1482–1495.

Ying, Q.-L., Wray, J., Nichols, J., Batlle-Morera, L., Doble, B., Woodgett, J., Cohen, P., and Smith, A. (2008). The ground state of embryonic stem cell self-renewal. Nature *453*, 519–523.

Ying, Q.L., Nichols, J., Chambers, I., and Smith, A. (2003). BMP induction of Id proteins suppresses differentiation and sustains embryonic stem cell self-renewal in collaboration with STAT3. Cell *115*, 281–292.

Yuan, J., Mehta, P.P., Yin, M.J., Sun, S., Zou, A., Chen, J., Rafidi, K., Feng, Z., Nickel, J., Engebretsen, J., et al. (2011). PF-04691502, a potent and selective oral inhibitor of PI3K and mTOR kinases with antitumor activity. Mol. Cancer Ther. *10*, 2189–2199.

Yusa, K., Zhou, L., Li, M.A., Bradley, A., and Craig, N.L. (2011). A hyperactive piggyBac transposase for mammalian applications. Proc. Natl. Acad. Sci. USA *108*, 1531–1536.